

FoundPose: Unseen Object Pose Estimation with Foundation Features

Evin Pinar Örnek^{1,2} Yann Labbé³ Bugra Tekin³ Lingni Ma³
 Cem Keskin³ Christian Forster³ Tomas Hodan³

¹Technical University of Munich ²Munich Center for Machine Learning ³Reality Labs at Meta

Abstract

We propose *FoundPose*, a method for 6D pose estimation of unseen rigid objects from a single RGB image. The method assumes that 3D models of the objects are available but does not require any object-specific training. This is achieved by building upon DINOv2, a recent vision foundation model with impressive generalization capabilities. An online pose estimation stage is supported by a minimal object representation that is built during a short onboarding stage from DINOv2 patch features extracted from rendered object templates. Given a query image with an object segmentation mask, *FoundPose* first rapidly retrieves a handful of similarly looking templates by a DINOv2-based bag-of-words approach. Pose hypotheses are then generated from 2D-3D correspondences established by matching DINOv2 patch features between the query image and a retrieved template, and finally optimized by featuremetric refinement. The method can handle diverse objects, including challenging ones with symmetries and without any texture, and noticeably outperforms existing RGB methods for coarse pose estimation in both accuracy and speed on the standard BOP benchmark. With the featuremetric and additional MegaPose refinement, which are demonstrated complementary, the method outperforms all RGB competitors. Source code is at: [evinpinar.github.io/foundpose](https://github.com/evinpinar/foundpose).

1. Introduction

Image-based estimation of the 6D object pose (3D rotation and 3D translation) is a crucial research problem in the field of spatial AI. In robotics, for example, the information about object poses allows a robot to act upon the objects which enables fully automated solutions for warehouse operation or assembly. In mixed reality applications, this information unlocks physical interaction with replicas of real-world objects, such as a computer keyboard for effective text input when fully immersed.

In this work, we address the problem of model-based 6D pose estimation of *unseen* objects. We assume that 3D models of the target objects are available and that budget for onboarding the objects is limited (*e.g.*, not sufficient for rendering a large-scale dataset and training a neural network). This is a practical problem setup for many applications since efficient object onboarding is often a key requirement and 3D object models can be obtained from the manufacturer or readily reconstructed [59, 76, 99].

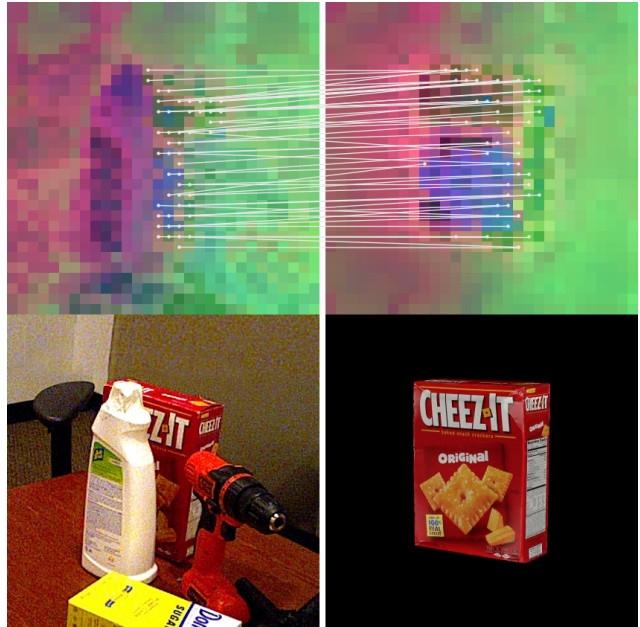


Figure 1. **Standing on the shoulders of DINOv2.** Patch features from the DINOv2 foundation model (top) are the key enabler of FoundPose. Without any training, a new object is onboarded just by rendering simple templates showing the object in different orientations, and by constructing a minimal feature representation that can support online pose estimation. Thanks to the generalization capability of DINOv2 features, it is possible to estimate the pose by direct feature matching between a query (left) and a retrieved template (right), despite the real-to-synthetic domain gap.

The very first methods for object pose estimation can in fact handle unseen objects. These methods rely on matching hand-crafted image features [50, 77, 78] or template matching [29, 58] and do not require any training. Later, with the rise of machine learning techniques in computer vision, most object pose estimation methods started to rely on deep neural networks. This shift brought a significant improvement in pose estimation accuracy [89] but limited generalization capability as large numbers of training images and a long training process are typically necessary for a new object instance or category. As a result, majority of these methods focus on a small set of object instances or categories. Only recently, with the accuracy scores of seen object pose estimation slowly saturating, the research

field started to focus again on unseen objects, with the first attempts achieving noticeably lower accuracy scores while being computationally more demanding [11, 34, 41, 82].

With their impressive generalization capabilities, foundation models [7] provide a solid ground for solving the problem at hand. Models such as DINOv2 [14, 65], CLIP [75] or ALIGN [37] have been successfully applied on various vision tasks without any fine-tuning [23, 56, 60, 97]. For example, the CNOS [60] method for segmentation of unseen objects, which leverages DINOv2 [14, 65] and Segment Anything [40], outperforms Mask R-CNN [25] without any training on the target objects.

Inspired by these success stories, we propose FoundPose, a method for model-based pose estimation of unseen objects that revisits classical computer vision techniques with the power of DINOv2, *without requiring any training*. Given an object segmentation mask from CNOS [60], we first rapidly retrieve a small set of similarly looking templates using bag-of-words descriptors [84], which are constructed from DINOv2 patch descriptors. For each retrieved template, we establish 2D-3D correspondences by matching DINOv2 patch descriptors of the query image and the template, and estimate a pose hypothesis by PnP-RANSAC [20, 43]. Finally, we refine the best hypothesis by featuremetric alignment. As demonstrated in our experiments, FoundPose works on diverse objects, including challenging objects with symmetries and without any texture.

In this work, we make the following contributions:

1. *A practical method for unseen object pose estimation* which demonstrates the effectiveness of DINOv2 for this task by outperforming existing methods on the BOP benchmark [34] in both accuracy and speed, without any training.
2. *A rapid template retrieval approach* which is based on visual words constructed from DINOv2 patch descriptors, is robust to partial object occlusions, and considerably simplifies the subsequent problem of establishing 2D-3D correspondences.
3. *A minimal template-based object representation* which is fast to build (requiring only several hundreds of rendered object templates), can effectively support online pose estimation, and has a low storage footprint enabling to scale to large numbers of objects (only bag-of-words descriptors and patch descriptors registered in 3D are stored).
4. *A featuremetric pose refinement approach* which is effective in reducing discrepancy in 2D-3D correspondences due to coarse patch sampling, and complementary to the MegaPose refiner (achieving more together than any of them alone).

2. Related work

This paper builds on over 60 years of research in object pose estimation, and on the recent large-scale vision foundation models.

Pose estimation of rigid objects. Estimating the 6D pose of a rigid object with a known 3D model from a single image is one of the oldest computer vision problems [77]. It was originally addressed by establishing 2D-3D correspondences using locally invariant features [13, 50, 77, 78], or by template matching using a global descriptor of the object appearance [29, 58]. Several

techniques to build local and global descriptors have been proposed in the literature. The first descriptors were manually designed and relied on intensity edges [19, 36, 49, 93], raw pixels [6, 55, 58, 64, 78] or image gradients [28, 29, 51]. Methods based on hand-crafted features have been progressively replaced and outperformed [32–34] by deep neural networks [30, 35, 46, 68–70, 85, 90, 91, 98, 102]. State of the art methods [34, 89, 96] typically do not rely on explicit feature representation and instead directly regress either the absolute [39, 96, 100] or relative pose [41, 42, 45, 53]. Methods based on direct absolute pose regression are trained for specific object instances or categories and do not generalize to unseen objects. Methods based on direct relative pose estimation usually rely on render-and-compare [45], which requires large amounts of synthetic images showing diverse objects to achieve generalization capabilities [41]. We build on earlier works on template matching and correspondence estimation, but use features extracted with a pre-trained DINOv2 model [65] instead of hand-crafted features. Our method does not require any training and can be directly applied to any object.

Pose estimation of *unseen* rigid objects. Motivated by practical applications, several methods that can be deployed to new objects without re-training have been proposed. Some of the methods address unseen object pose estimation without a 3D model [26, 27, 47, 87] by capturing multiview reference views and relative poses. Others propose learning local or global descriptors that can generalize to unseen objects. For example [61, 82, 88, 92, 98] learn global descriptors for template matching using contrastive learning [61, 82, 92, 98] or an auto-encoder [88]. A sparse set of generic 3D keypoints is predicted in [73, 74], [82] uses a network to predict dense correspondences, and [101] directly predicts the 3D object orientation. Other methods rely on depth measurements [4, 11, 63, 67]. In this work, we consider the more challenging scenario where only RGB images are available.

The state of the art [34] methods [41, 57] for 6D pose estimation of unseen objects rely on a three-stage approach as follows (1) 2D detection using CNOS [60], (2) a coarse pose is estimated by a neural network that predicts similarity between templates and the cropped input image, and (3) pose refinement by a regression network based on the render-and-compare strategy [24, 42, 45, 57, 62]. These methods achieve generalization to novel objects by training on millions of images showing thousands of different objects. Such datasets [41] can only be obtained in simulation, which exposes them to the synthetic-to-real domain gap. Our method leverages a foundation model, and without any re-training, significantly outperforms previous coarse pose estimation strategies in terms of accuracy and runtime, and achieves the state of the art when combined with the refinement network of MegaPose [41]. Concurrent to our work is ZS6D [3] which also uses a foundation model for pose estimation and to which we compare in Sec. 4.

Foundation models on related tasks. A foundation model is a machine-learning model trained on broad data using self-supervised learning that can be adopted to a wide range of downstream tasks [7]. Foundation models initially appeared in Natural Language Processing (NLP) with examples such as

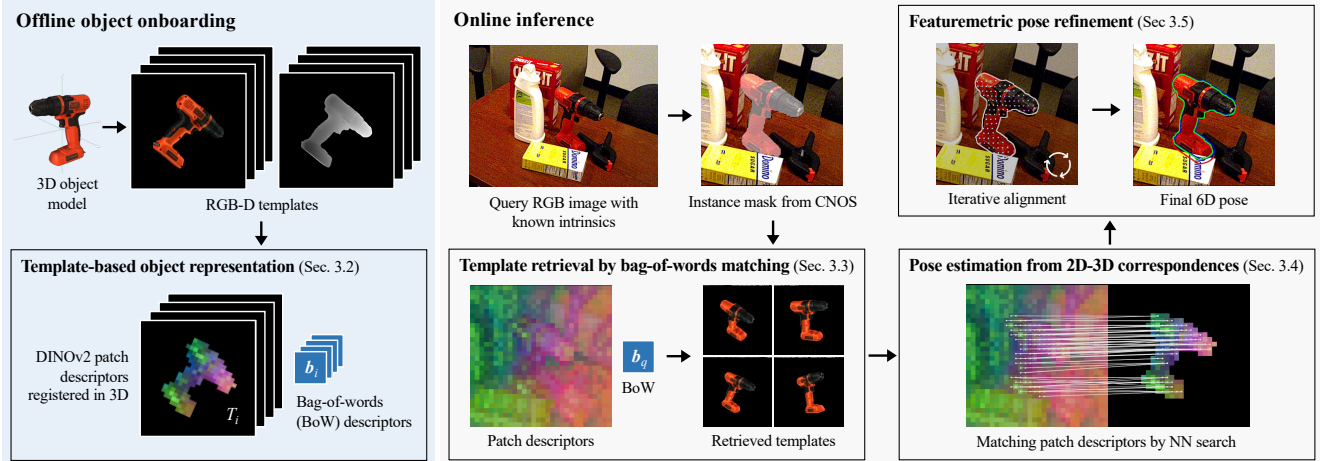


Figure 2. **FoundPose overview.** During a short onboarding stage, we render RGB-D templates showing the object in different orientations, extract DINOv2 patch descriptors [14, 65] from the RGB channels and register the descriptors in 3D using the depth channel. At inference time, we crop the RGB query image around the object mask predicted by CNOS [60] and retrieve a small set of most similar templates using a bag-of-words approach (with words defined by k -means clusters of patch descriptors from all templates). For each retrieved template, a pose hypothesis is generated by PnP-RANSAC [20, 43] from 2D-3D correspondences established by matching DINOv2 patch descriptors of the image crop and the template. Finally, the pose hypothesis with the highest number of inlier correspondences is refined by featuremetric alignment and reported as the final pose estimate.

BERT [15] or GPT-3 [9]. In computer vision, foundation models include CLIP [12, 75], ALIGN [37], iBOT [104], ImageBind [22], DINOv1 [10], and DINOv2 [65]. The amount of data [65, 80] used to train these models and their performance [65] on downstream tasks are constantly growing. The models have achieved results on-par or better than supervised models for several fundamental computer vision tasks, such as image classification [10, 12, 65], semantic segmentation [56], object discovery [66, 83, 97], and depth estimation [65]. DINOv2, which is based on a Vision Transformer architecture [16] and trained in self-distillation fashion, has been successfully employed in several works. Thanks to the attention architecture which meets the global context with local image features, it has been shown to encode both the high spatial information about the object parts as well as semantic information such as object categories [2]. It has been successfully used in zero-shot setups, *i.e.*, without any training, for establishing semantic correspondences [2, 23, 48, 103]. Building on top of these recent insights about foundation models, we present an approach that uses DINOv2 for the task of 6D pose estimation of unseen objects and improves the state of the art.

3. FoundPose

In this section we describe FoundPose, the proposed method for unseen object pose estimation. We first provide a high-level overview of the method in Sec. 3.1 and then focus on the key components and rationale of our design choices in Sec. 3.2–3.5.

3.1. Method overview

Problem definition. We consider the problem of estimating the 6D pose of rigid objects from a single RGB image with known intrinsics. The objective is to estimate the pose of all instances of target objects that are visible in the image. We assume that

the only information provided for the target objects are their 3D mesh models, and there is only a limited budget for onboarding the objects, *i.e.*, for preparing object representations that can be used for pose estimation. We assume that segmentation masks of the target object instances, together with per-mask object identity, are provided at inference time. In our experiments, we obtain the masks by CNOS [60], a recent method for segmentation of unseen objects that similarly is based on DINOv2 and requires only 3D models for onboarding the objects.

Onboarding and inference. During an offline onboarding stage, we render templates showing 3D object models in different orientations. From each template, we extract DINOv2 descriptors of image patches and register the descriptors in 3D, *i.e.*, each patch descriptor is associated with the corresponding 3D location in the object model space (Sec. 3.2). At inference time, given a segmentation mask of an object instance, we crop the image region around the mask, extract DINOv2 patch descriptors of the crop, and use them with a bag-of-words retrieval technique to efficiently identify a small set of templates that show the object in orientations similar to the observation (Sec. 3.3). For each retrieved template, we establish 2D-3D correspondences by matching DINOv2 patch descriptors from the crop against patch descriptors of the templates registered in 3D and generate a pose hypothesis using the PnP-RANSAC algorithm (Sec. 3.4). Finally, we refine the best pose hypothesis by featuremetric alignment, an optimization-based algorithm inspired by photometric alignment that operates on features (Sec. 3.5). The pipeline of the method is shown in Fig. 2.

3.2. Template-based object representation

Template generation. Given a texture-mapped 3D object model, we render n RGB-D templates showing the model under different orientations. The orientations are sampled to uniformly cover the

$SO(3)$ group of 3D rotations [1], and the model is rendered using a standard rasterization technique [81] with a black background and fixed lighting. The size of templates is $S \times S$ pixels and the objects are rendered such as the longer side of their 2D bounding box is δS pixels long, with $\delta < 1$. At inference, we generate crops of the query image with the same size and padding (to allow for errors of segmentation masks around which we crop the image).

Patch descriptors registered in 3D. For each RGB-D template with an index $t \in \{1, \dots, n\}$, we split the RGB channels into m non-overlapping patches of 14×14 pixels and calculate their patch descriptors $\{\mathbf{p}_{t,i}\}_{i=1}^m$. A patch descriptor is calculated as $\mathbf{p}_{t,i} = \phi_d(\mathbf{p}'_{t,i})$, where $\mathbf{p}'_{t,i}$ is the raw patch descriptor extracted by DINOv2 and $\phi_d: \mathbb{R}^r \mapsto \mathbb{R}^d$ projects the r dimensional raw descriptor to the top d PCA components calculated from valid patch descriptors of all n templates. A patch is considered valid if its 2D center falls inside the object mask and the PCA-based dimensionality reduction is applied to increase efficiency. Then we represent a template t by a set $T_t = \{(\mathbf{p}_{t,j}, \mathbf{x}_j) \mid j \in M\}$, where M are indices of valid patches, \mathbf{x}_j is a 3D location in the object model space whose 2D projection is at the center of patch j . The 3D locations, which are calculated from the depth channel of the template and known camera intrinsics, enable establishing 2D-3D correspondences at inference.

Bag-of-words descriptors. At onboarding, we also pre-calculate bag-of-words descriptors of all templates to enable efficient template retrieval at inference using the classical bag-of-words image retrieval technique [72, 84], which mimics text-retrieval systems with the analogy of visual words. Specifically, we define visual words as the centroids of k -means clusters of patch descriptors extracted from all templates of an object. To calculate the bag-of-words descriptor of a template t , we assign patch descriptors from the template representation T_t to the nearest visual words and describe the template by a vector $\mathbf{b}_t = (b_1, b_2, \dots, b_k)$. This vector consists of weighted word frequencies defined as $b_i = \frac{n_{i,t}}{n_t} \log \frac{N}{n_i}$, where $n_{i,t}$ is the number of occurrences of word i in template t , n_t is the total number of words in template t , n_i is the number of occurrences of word i in all N templates. The first term ($\frac{n_{i,t}}{n_t}$) weights words that occur often in a particular template and therefore describe the template well, while the second term ($\log \frac{N}{n_i}$) downweights words that occur often in any template. As visual words generated by clustering may suffer from quantization errors, we follow [72, 94] and soft-assign each patch descriptor to several nearest words with weights defined by $\exp -\frac{d^2}{2\sigma^2}$, where d is the Euclidean distance of the descriptor from the word and σ is a parameter of the method.

3.3. Template retrieval by bag-of-words matching

Perspective cropping. At inference, we start by cropping the image region around a given object segmentation mask. To minimize perspective distortion and achieve a crop that resembles a template, we generate the crop by warping the query image to a virtual pinhole camera focused at the segmentation mask. The virtual camera is constructed such as its optical axis is passing through the center of the 2D bounding box of the mask, the

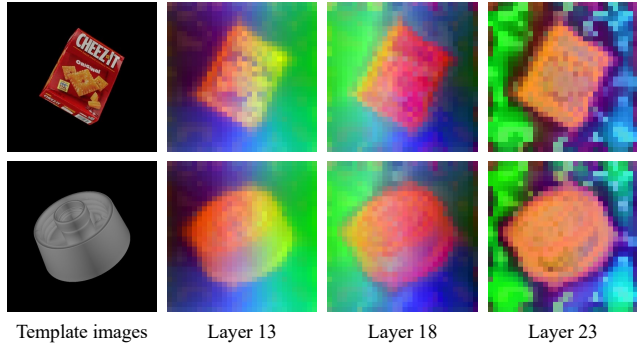


Figure 3. **Visualization of DINOv2 patch descriptors.** Shown are top three PCA components of patch descriptors extracted at different layers of DINOv2 ViT-L [14] from templates of a textured object from YCB-V [100] and a symmetric and texture-less object from T-LESS [31]. As observed in [2] and also clearly visible in these visuals, patch descriptors contain gradually less positional and more semantic information when going from shallower to deeper layers. FoundPose performs the best with descriptors from layer 18, which presumably provides the right information mix. The positional information is important for producing geometrically consistent correspondences when the semantic information is not discriminative due to symmetries or a lack of texture.

viewport size is $S \times S$ pixels, and the longer side of the warped 2D bounding box is δS pixels long.

Retrieving similar templates. To retrieve a small set of templates, we calculate the bag-of-words descriptor of the crop (as in Sec. 3.2) and calculate its cosine similarity (*i.e.*, normalized scalar product) with bag-of-words descriptors of all object templates. We select h templates with the highest cosine similarity, which provide approximate hypotheses on the object orientation for the subsequent pose estimation stage. This retrieval technique is robust to partial occlusions and remarkably efficient.

Since the bag-of-words descriptor represents an image as a bag of unordered visual words, the retrieval can be typically improved by re-ranking the results with a spatial verification stage [71]. However, in our case, a similar verification is implicitly done by the subsequent PnP-RANSAC (spatially consistent correspondences are expected to yield a better pose estimate) and bags of words are not completely unordered as the used patch descriptors from an intermediate DINOv2 layer, from which the words are constructed, contains 2D positional information.

3.4. Pose estimation from 2D-3D correspondences

Crop-to-template patch matching. For each retrieved template t , we match patch descriptors from the image crop to the nearest (in terms of the Euclidean distance) descriptors from T_t and establish 2D-3D correspondences $C_t = \{(\mathbf{u}_i, \mathbf{x}_i)\}_{i=1}^m$, where \mathbf{u}_i is the 2D center of a patch in the query image and \mathbf{x}_i is the 3D location associated with the matched patch descriptor from T_t .

Establishing 2D-3D correspondences by crop-to-template patch matching is a considerably simpler problem than exhaustive matching against patch descriptors from all templates, which would be necessary without the template retrieval. Moreover, we demonstrate that the template-based approach can effectively

handle arbitrary objects, including challenging objects with symmetries and without a significant texture. The ambiguity of 2D-3D correspondences [30], for which such objects are notoriously known, is eliminated by (1) restricting the candidate descriptors to ones from a single template and (2) using patch descriptors from intermediate layers of DINOv2 that contain both semantic and 2D positional information [2] (Fig. 3). The positional information is the key for producing geometrically consistent correspondences when the semantic information is not discriminative due to symmetries or a lack of texture.

Pose fitting. An object pose $(\mathbf{R}_t, \mathbf{t}_t)$, defined by a 3D rotation \mathbf{R}_t and 3D translation \mathbf{t}_t from the model space to the camera space, is estimated for each retrieved template t from 2D-3D correspondences C_t by solving the Perspective- n -Point (PnP) problem. We solve this problem by the EPnP algorithm [43] combined with the RANSAC fitting scheme [20] for robustness. In this scheme, PnP is solved repeatedly on a randomly sampled minimal set of 4 correspondences and the final output is defined by the pose hypothesis with the highest quality, which we define by the number of inlier correspondences [20]. From the set of h poses estimated from the h retrieved templates, the pose with the highest quality is selected as the final coarse pose estimate $(\mathbf{R}_c, \mathbf{t}_c)$.

3.5. Featuremetric pose refinement

Featuremetric alignment. The coarse pose $(\mathbf{R}_c, \mathbf{t}_c)$ is further refined by Levenberg-Marquardt (L-M) [44, 54], an iterative non-linear optimization algorithm. Each L-M iteration updates the pose parameters by a gradient-descent step minimizing a real-valued cost, while adaptively selecting between the first and second order gradients depending on the cost value. We initialize the optimization with the coarse pose $(\mathbf{R}_c, \mathbf{t}_c)$ and obtain a refined pose $(\mathbf{R}_r, \mathbf{t}_r)$ by minimizing a featuremetric error:

$$(\mathbf{R}_r, \mathbf{t}_r) = \underset{(\mathbf{R}, \mathbf{t})}{\operatorname{argmin}} \sum_{(\mathbf{p}_i, \mathbf{x}_i) \in T_t} \rho \left(\mathbf{p}_i - \mathbf{F}_q \left(\pi(\mathbf{R}\mathbf{x}_i + \mathbf{t})/s \right) \right),$$

where ρ is a robust cost function by Barron [5], $(\mathbf{p}_i, \mathbf{x}_i) \in T_t$ is a descriptor and the corresponding 3D location of patch i from template t , and $\pi: \mathbb{R}^3 \mapsto \mathbb{R}^2$ represents the 2D projection. The feature map $\mathbf{F}_q \in \mathbb{R}^{a \times a \times d}$ is obtained by stacking the patch descriptors of the query image and is sampled with bilinear interpolation at normalized 2D projections. The spatial resolution of the feature map is $a \times a$ with $a = S/s$, where $s \times s$ is the patch size. Note that a similar featuremetric alignment was applied in several works [79, 95], typically in combination with features trained specifically for L-M. In our work, we apply optimization directly on DINOv2 features, without any training.

Reducing 2D-3D discrepancy. The 2D-3D correspondences are established by matching patch descriptors extracted on a regular grid in the query image given by the 2D patch centers. Such a coarse sampling may reduce the accuracy of pose estimates as the centers of matched patches may not be aligned with 2D projections of the same 3D points. To compensate for the potential discrepancy, we refine the pose estimates by aligning template patches to their optimal locations in the query image. Another possible approach to reduce the discrepancy is to

increase spatial density of the extracted patch descriptors, which could be achieved, *e.g.*, by splitting the image into overlapping patches [2]. However, this approach reduces efficiency while not improving accuracy of our method.

4. Experiments

In this section, we compare the accuracy and speed of FoundPose with the state-of-the-art methods evaluated on the BOP benchmark [32–34, 89] and present ablation experiments.

4.1. Experimental setup

Evaluation protocol. We follow the protocol of the BOP Challenge 2019–2023 [33]. In summary, a method is evaluated on the 6D object localization problem, and the error of an estimated pose w.r.t. the ground-truth pose is calculated by three pose-error functions: Visible Surface Discrepancy (VSD) treats ambiguous poses as equivalent by considering only the visible object part, Maximum Symmetry-Aware Surface Distance (MSSD) considers a set of pre-identified global object symmetries and measures the surface deviation in 3D, and Maximum Symmetry-Aware Projection Distance (MSPD) considers the object symmetries and measures the perceivable deviation. An estimated pose is considered correct w.r.t. a pose-error function e , if $e < \theta_e$, where $e \in \{\text{VSD}, \text{MSSD}, \text{MSPD}\}$ and θ_e is the threshold of correctness. The fraction of annotated object instances for which a correct pose is estimated is referred to as Recall. The Average Recall w.r.t. a function e , denoted as AR_e , is defined as the average of the Recall rates calculated for multiple settings of the threshold θ_e and also for multiple settings of a misalignment tolerance τ in the case of VSD. The overall accuracy of a method is measured by the Average Recall: $\text{AR} = (\text{AR}_{\text{VSD}} + \text{AR}_{\text{MSSD}} + \text{AR}_{\text{MSPD}})/3$.

Datasets. The experiments are conducted on the seven core BOP datasets: LM-O [8], T-LESS [31], ITODD [18], HB [38], YCB-V [100], IC-BIN [17], and TUD-L [32]. The datasets feature 108 diverse objects ranging from texture-less and symmetric industrial objects (ITODD, T-LESS) to typical household objects. The images show scenes whose complexity varies from simple scenes with several isolated objects to challenging ones with multiple object instances and a high amount of clutter and occlusion. Only 3D object models and test images from these datasets were used for experiments with FoundPose, not the provided synthetic nor real training images since no training is required.

Compared methods. FoundPose is compared against RGB methods evaluated on the unseen object pose estimation task of the BOP Challenge 2023 [34], GenFlow [57] and MegaPose [41], along with OSOP [82] and ZS6D [3]. FoundPose, GenFlow, MegaPose and ZS6D use the same segmentation masks that were produced by CNOS [60] and provided to the challenge participants, while OSOP relies on a custom detector of unseen objects for LM-O, HB, and YCB-V, and on Mask R-CNN [25] trained for the specific objects for T-LESS (hence we do not include the T-LESS result). MegaPose consists of coarse pose estimation followed by a render-and-compare refiner. Besides variants of FoundPose where the coarse poses are refined by the

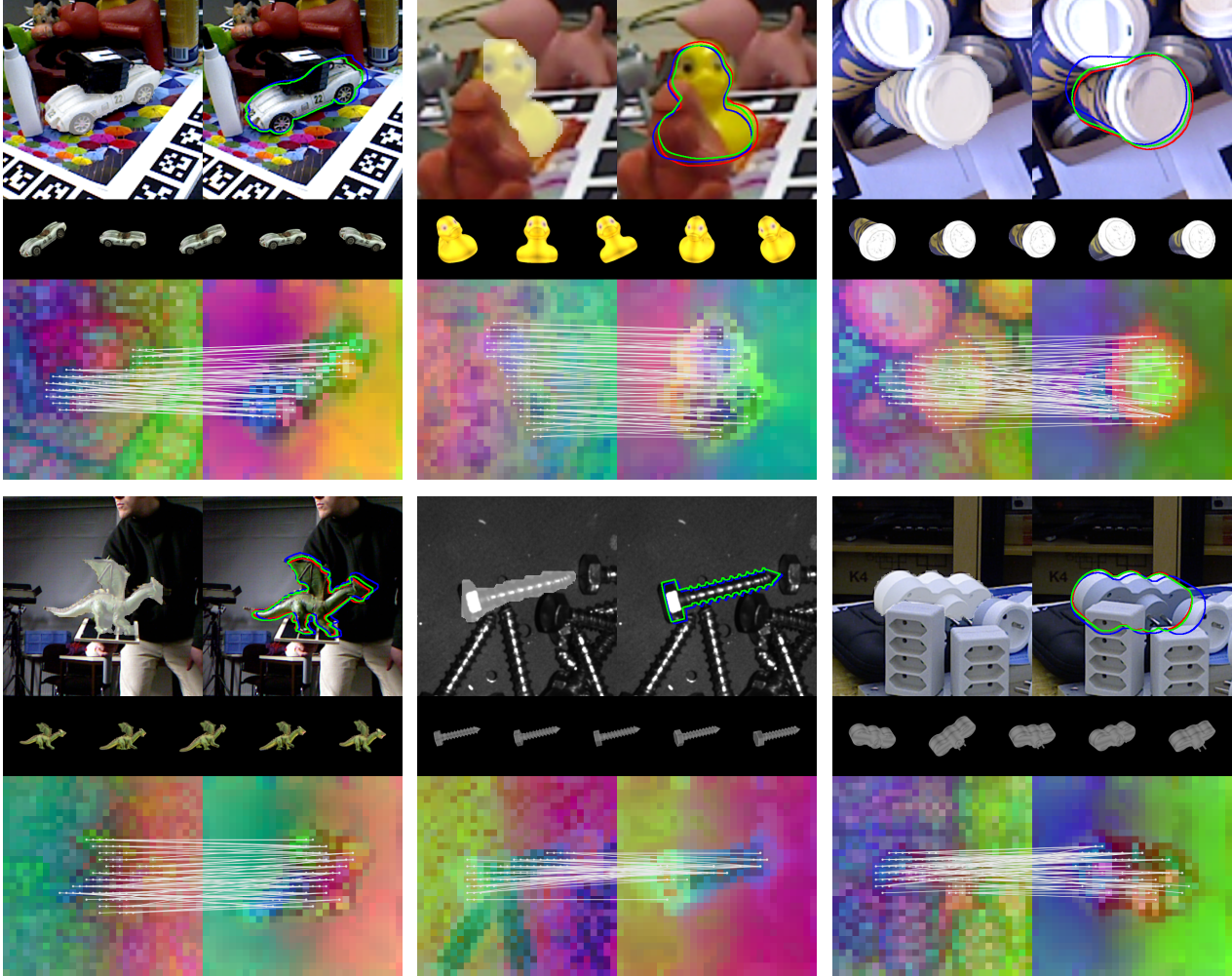


Figure 4. **Example FoundPose results** on HB, LM-O, IC-BIN, TUD-L, ITODD and T-LESS datasets. Each example shows the query image crop with the CNOS mask in white (top left), retrieved templates (middle row), matched patch descriptors of the crop and the template that led to a pose with the highest number of inlier correspondences (bottom row), and the ground-truth pose contour in red, the coarse pose in blue and the refined pose in green (top right). These examples demonstrate that FoundPose can handle a broad range of objects, including textured, texture-less and symmetric ones.

featuremetric refinement (Sec. 3.5), we evaluate variants where the coarse poses are refined by 5 iterations of the MegaPose refiner.

FoundPose parameters. For the presented experiments, we rendered 800 templates per object with approximately 25° angle between depicted object orientations. Decreasing the number of templates to 400 or increasing to 1600 influences memory requirements, but does not have a noticeable impact on accuracy or speed. We set the size of templates and of the query image crop to 420×420 px with $\delta = 0.6$. With the patch size of 14×14 px (for which DINOv2 is trained), we extract 30×30 patch descriptors from each template/crop and reduce their dimensionality by projecting them to top 256 PCA components. Unless stated otherwise, we use the output tokens from layer 18 of DINOv2 ViT-L/14 with registers [14] as the patch descriptors. Visual words for the bag-of-words template retrieval are defined per object by the centroids of 2048 k -means clusters of patch

descriptors from all templates of the object. The bag-of-words descriptors are constructed by soft-assigning each patch descriptor to 3 nearest words with $\sigma = 10$. For each query image crop, we retrieve 5 templates, and estimate the pose from 2D-3D correspondences (established between the query image crop and the template) by PnP -RANSAC running for up to 400 iterations with the inlier threshold set to 10 px. The featuremetric refinement is applied to the best coarse pose and runs until convergence for up to 30 iterations, with the Barron loss [5] parameters set to $\alpha = -5$ and $c = 0.5$. By default, the evaluated FoundPose variants use n CNOS masks per object, where n is the number of object instances to localize (provided as input in the 6D object localization task from BOP). The only exception are variants in the bottom part of Tab. 1 which use $5n$ CNOS masks per object. In these variants, the pose estimate with the best refinement score is selected as the final pose. When these variants use only n masks per object, the accuracy drops by 1–2 AR on all datasets.

Method	Pose refinement	LM-O	T-LESS	TUD-L	IC-BIN	ITODD	HB	YCB-V	Average	Time	
<i>Coarse pose estimation:</i>											
1	FoundPose	–	39.6	33.8	46.7	23.9	20.4	50.8	45.2	37.2	1.7
2	GenFlow [57]	–	25.0	<u>21.5</u>	<u>30.0</u>	<u>16.8</u>	<u>15.4</u>	28.3	27.7	<u>23.5</u>	<u>3.8</u>
3	MegaPose [41]	–	22.9	17.7	25.8	15.2	10.8	25.1	28.1	20.8	15.5
4	OSOP [82]	–	<u>31.2</u>	–	–	–	–	<u>49.2</u>	<u>33.2</u>	–	–
5	ZS6D [3]	–	29.8	21.0	–	–	–	–	32.4	–	–
<i>With pose refinement (a single hypothesis):</i>											
6	FoundPose	Featuremetric	39.5	39.6	56.7	28.3	26.2	58.5	49.7	42.6	2.6
7	FoundPose	MegaPose	<u>55.4</u>	51.0	63.3	<u>43.0</u>	<u>34.6</u>	<u>69.5</u>	66.1	<u>54.7</u>	<u>4.4</u>
8	FoundPose	Featuremetric + MegaPose	55.7	51.0	63.3	43.3	35.7	69.7	66.1	55.0	6.4
9	MegaPose [41]	MegaPose	49.9	<u>47.7</u>	<u>65.3</u>	36.7	31.5	65.4	<u>60.1</u>	50.9	31.7
<i>With pose refinement (multiple hypotheses):</i>											
10	FoundPose*	Featuremetric, 5 hyp.	42.0	43.6	60.2	30.5	27.3	53.7	51.3	44.1	7.4
11	FoundPose*	MegaPose, 5 hyp.	58.6	54.9	65.7	44.4	36.1	70.3	<u>67.3</u>	56.8	<u>11.2</u>
12	FoundPose*	Featuremetric + MegaPose, 5 hyp.	61.0	57.0	69.4	47.9	40.7	<u>72.3</u>	69.0	59.6	20.5
13	GenFlow [57]	GenFlow, 5 hyp.	56.3	52.3	68.4	45.3	39.5	<u>73.9</u>	63.3	57.1	20.9
14	GenFlow [57]	GenFlow, 16 hyp.	<u>57.2</u>	<u>52.8</u>	<u>68.8</u>	<u>45.8</u>	<u>39.8</u>	74.6	64.2	<u>57.6</u>	40.5
15	MegaPose [41]	MegaPose, 5 hyp.	56.0	50.7	68.4	41.4	33.8	70.4	62.1	54.7	47.4
16	MegaPose [41]	MegaPose, 10 hyp.	56.0	50.8	68.7	41.9	34.6	70.6	62.0	54.9	53.9

Table 1. **Performance on the seven core BOP datasets [89].** The table shows Average Recall (AR) scores per dataset, the average AR score, and the time to estimate poses of all objects in an image averaged over the datasets (in seconds). Methods for coarse pose estimation (without applying any refinement) are in the upper part, methods applying a refinement stage on a single coarse pose hypothesis are in the middle, and methods refining multiple coarse poses and reporting the top refined pose are at the bottom. The variants in the bottom part (marked with *) are run on top $5n$ CNOS segmentation masks per object, where n is the number of object instances to localize (see Sec. 4.1 for details on used FoundPose parameters).

4.2. Main results

Accuracy. Among methods that do not apply any refinement stage, FoundPose (without the featuremetric refinement) produces significantly more accurate poses than the competitors, achieving +14 and +17 AR on the seven BOP datasets on average w.r.t. the coarse versions of GenFlow [57] or MegaPose [41] (rows 1–3 in Tab. 1). The featuremetric refinement brings an extra improvement of +5 AR on average (rows 1 vs 6). At an additional computational cost, a large improvement of +17 AR (rows 1 vs 7) can be achieved if the coarse poses from FoundPose are refined by the iterative render-and-compare approach from MegaPose, which is trained on 2M+ synthetic images of diverse objects and proven remarkably effective. When initiated with coarse poses from FoundPose, the MegaPose refiner achieves +4 higher AR score than when initiated with poses from the original coarse pose estimation stage of MegaPose (rows 7 vs 9). Additional improvements at additional computational cost can be achieved if the refinement is applied to multiple pose hypotheses and the top refined pose is reported as the final estimate (rows 10–16). We achieve the overall best average AR score of 59.6 AR when top 5 pose hypotheses are optimized with the featuremetric refinement followed by the MegaPose refinement. On both the single and multi hypotheses setups, the combination of the two refinement approaches achieves the best scores (rows 8 and 12), suggesting their complementarity. This entry outperforms multi-hypotheses versions of MegaPose and GenFlow, including the winning RGB method from BOP Challenge 2023 [34] (row 14).

Speed. The presented variants of FoundPose are the most accurate and fastest entries in all three categories evaluated in Tab. 1.¹ Notably, the coarse pose estimation stage from FoundPose is significantly faster (1.7 vs 15.5 s) and more accurate than the coarse render-and-compare stage from MegaPose (rows 1 vs 3). The FoundPose variants provide a spectrum of trade-offs between speed and accuracy, with the faster variants (rows 1 and 6) being relevant for online applications such as robotic manipulation, while the more accurate variants being relevant for offline applications such as ground-truth object pose annotation for training supervised methods [89]. The trade-off can be further controlled by, *e.g.*, the template size, the number of PCA components for dimensionality reduction of the patch descriptors, or by different types of the DINOv2 backbone – row 3–4 in Tab. 2 shows that FoundPose runs at around 1.3 s per image if the ViT-L backbone (used for results in Tab. 1) is replaced with the smaller ViT-S. Note that the reported times include also the CNOS segmentation stage that takes around 0.3 s per image.

4.3. Ablation experiments.

Feature extractors. Tab. 2 (rows 1–7) evaluates the performance of FoundPose (without the featuremetric refinement) with different patch descriptors. We achieve the best pose accuracy when we use the output tokens of layer 18 (out of 23) from the DINOv2 ViT-L model with registers [14] as the patch descriptors.

¹OSOP [82] has a light version that runs at < 1 s per image, but has lower accuracy scores (-3 AR) than the entry in Tab. 1, which takes 5–12 s per image.

	LM-O	T-LESS	TUD-L	IC-BIN	ITODD	HB	YCB-V	Average	Time
<i>Backbones for extraction of image patch descriptors:</i>									
1 DINOv2 ViT-L – layer 18	39.6	33.8	46.7	23.9	20.4	50.8	45.2	37.2	1.7
2 DINOv2 ViT-L – layer 23	23.2	22.8	31.2	10.3	9.7	33.0	34.0	23.5	1.5
3 DINOv2 ViT-S – layer 9	34.0	31.6	42.7	21.7	16.8	46.8	44.7	34.0	1.3
4 DINOv2 ViT-S – layer 11	22.8	24.2	29.8	11.9	10.5	30.4	36.4	23.7	1.3
5 SAM ViT-L [40] – layer 23	2.2	12.8	9.2	7.5	6.0	10.6	26.9	10.7	3.4
6 DenseSIFT – step size 7px	3.2	2.6	6.5	10.5	2.9	5.6	22.2	7.6	1.4
7 S2DNet [21]	0.8	1.2	0.8	1.4	1.2	1.2	1.3	1.1	1.8
<i>Template retrieval by matching <code>cls</code> token from layer 18 of DINOv2 ViT-L:</i>									
8 Retrieval by <code>cls</code> token	19.9	17.8	24.6	10.3	13.6	17.7	23.6	18.2	1.6
9 Retrieval by <code>cls</code> token with black bg.	25.5	26.2	30.3	16.7	13.6	29.3	34.4	25.1	1.6
<i>Other ablations:</i>									
10 Pose given by the top matched template	20.3	18.5	23.0	12.8	12.4	19.6	17.6	17.7	1.0
11 Ground-truth instead of CNOS masks	45.6	53.1	57.1	30.6	–	–	50.9	–	–

Table 2. **Ablation experiments.** We analyze different backbones for extraction of image patch descriptors (rows 1–7), compare our bag-of-words template matching with alternative approaches based on matching the `cls` token (rows 1 vs 8 and 9), evaluate our template matching approach by taking the pose associated with the top template as the final pose estimate (row 10), and show the accuracy of coarse poses from FoundPose when ground-truth masks are used instead of the CNOS masks [60] (row 11; ground-truth annotations for ITODD and HB are not publicly available).

We observed also qualitatively that this layer provides a good balance between the positional and semantic information – the resulting correspondences are more geometrically consistent while more discriminative than correspondences obtained using later and earlier layers respectively (Fig. 3).

Furthermore, we evaluate FoundPose with patch descriptors extracted from layer 23 of the SAM ViT-L model [40], from the last backbone layers of the feature matching pipelines LoFTR [86] and S2DNet [21], from the last layer of the CLIP image encoder [75], and with patch descriptors defined by the classical SIFT descriptor [52] calculated on a regular 2D grid with the cell size of 7 px. In case of S2DNet, patch descriptors were obtained by sampling the last CNN feature map. All method parameters were fixed in these experiments, only the patch descriptors were different. As shown in Tab. 2, patch descriptors from DINOv2 are the key enabler of FoundPose, yielding significantly higher accuracy than the alternatives (we only show performance of the better alternatives).

Template retrieval. Next, on rows 8–9 in Tab. 2, we evaluate the proposed bag-of-words template retrieval approach against an alternative based on matching the `cls` token from DINOv2. In this alternative, we use the `cls` token from layer 18 of DINOv2 ViT-L as the template & crop descriptor, and retrieve templates whose descriptors have the highest cosine similarity with the descriptor of the query image crop. A similar approach is used in ZS6D [3] for initial viewpoint estimation and in CNOS [60] for object identification. Compared to the bag-of-words descriptor constructed from patch descriptors, we observed that the `cls` token is less robust to occlusions and contains a limited information about the object pose (as also shown in Fig. 5 in [60]). To avoid influence of the background on the `cls` token, we additionally evaluate a variant where

pixels outside the object mask are made black, as in [3, 60]. As shown on rows 8 vs 9 in Tab. 2, this modification improves the performance of the `cls`-based approach, but is still far from the performance of our bag-of-words approach (row 1). When tried with the `cls` token from layer 23, the alternative retrieval approach achieved even lower accuracy.

We further analyze the quality of templates retrieved by the bag-of-words approach by evaluating the object pose associated with the top retrieved template. The pose from the template is adjusted such as the 2D bounding circle of the object is aligned with the 2D bounding circle of the object segmentation mask in the query image. This approach is surprisingly effective, reaching accuracy close to the coarse poses from MegaPose while being 15 times faster (row 10 in Tab. 2 vs row 3 in Tab. 1).

Ground-truth segmentation masks. A common source of FoundPose failure cases are erroneous object segmentation masks. When the ground-truth masks are used instead of the masks predicted by CNOS [60], FoundPose achieves a large improvement of +6–19 AR (rows 1 vs 11 in Tab. 2).

5. Conclusion

We have proposed a practical method for model-based pose estimation of unseen objects which demonstrates the effectiveness of features from the DINOv2 foundation model for this task. The method can handle a broad range of objects, including texture-less and symmetric objects, can scale to large numbers of objects thanks to a minimal object representation, and is computationally efficient, mostly thanks to the bag-of-words template retrieval which simplifies the subsequent process of establishing 2D-3D correspondences by providing a small set of reliable templates. Without any object-specific training, variants of FoundPose outperform existing RGB methods on the BOP benchmark.

References

- [1] Marc Alexa. Super-fibonacci spirals: Fast, low-discrepancy sampling of $SO(3)$. *CVPR*, 2022. 4
- [2] Shir Amir, Yossi Gandelsman, Shai Bagon, and Tali Dekel. Deep vit features as dense visual descriptors. *ECCVW*, 2022. 3, 4, 5
- [3] Philipp Ausserlechner, David Habeger, Stefan Thalhammer, Jean-Baptiste Weibel, and Markus Vincze. ZS6D: Zero-shot 6D object pose estimation using vision transformers. *arXiv preprint arXiv:2309.11986*, 2023. 2, 5, 7, 8
- [4] Vassileios Balntas, Andreas Doumanoglou, Caner Sahin, Juil Sock, Rigas Kouskouridas, and Tae-Kyun Kim. Pose guided RGBD feature learning for 3D object pose estimation. *ICCV*, 2017. 2
- [5] Jonathan T. Barron. A general and adaptive robust loss function. *CVPR*, 2019. 5, 6
- [6] Herbert Bay, Tinne Tuytelaars, and Luc Van Gool. SURF: Speeded up robust features. *ECCV*, 2006. 2
- [7] Rishi Bommasani, Drew A Hudson, Ehsan Adeli, Russ Altman, Simran Arora, Sydney von Arx, Michael S Bernstein, Jeannette Bohg, Antoine Bosselut, Emma Brunskill, et al. On the opportunities and risks of foundation models. *arXiv preprint arXiv:2108.07258*, 2021. 2
- [8] Eric Brachmann, Alexander Krull, Frank Michel, Stefan Gumhold, Jamie Shotton, and Carsten Rother. Learning 6D object pose estimation using 3D object coordinates. *ECCV*, 2014. 5
- [9] Tom Brown, Benjamin Mann, Nick Ryder, Melanie Subbiah, Jared D Kaplan, Prafulla Dhariwal, Arvind Neelakantan, Pranav Shyam, Girish Sastry, Amanda Askell, et al. Language models are few-shot learners. *Advances in neural information processing systems*, 2020. 3
- [10] Mathilde Caron, Hugo Touvron, Ishan Misra, Hervé Jégou, Julien Mairal, Piotr Bojanowski, and Armand Joulin. Emerging properties in self-supervised vision transformers. *ICCV*, 2021. 3
- [11] Jianqiu Chen, Mingshan Sun, Tianpeng Bao, Rui Zhao, Liwei Wu, and Zhenyu He. ZeroPose: CAD-model-based zero-shot pose estimation. *arXiv preprint arXiv:2305.17934*, 2023. 2
- [12] Mehdi Cherti, Romain Beaumont, Ross Wightman, Mitchell Wortsman, Gabriel Ilharco, Cade Gordon, Christoph Schuhmann, Ludwig Schmidt, and Jenia Jitsev. Reproducible scaling laws for contrastive language-image learning. *CVPR*, 2023. 3
- [13] Alvaro Collet, Manuel Martinez, and Siddhartha S. Srinivasa. The MOPED framework: Object recognition and pose estimation for manipulation. *IJRR*, 2011. 2
- [14] Timothée Darcet, Maxime Oquab, Julien Mairal, and Piotr Bojanowski. Vision transformers need registers. *arXiv preprint arXiv:2309.16588*, 2023. 2, 3, 4, 6, 7
- [15] Jacob Devlin, Ming-Wei Chang, Kenton Lee, and Kristina Toutanova. BERT: Pre-training of deep bidirectional transformers for language understanding. *ACL*, 2019. 3
- [16] Alexey Dosovitskiy, Lucas Beyer, Alexander Kolesnikov, Dirk Weissenborn, Xiaohua Zhai, Thomas Unterthiner, Mostafa Dehghani, Matthias Minderer, Georg Heigold, Sylvain Gelly, Jakob Uszkoreit, and Neil Houlsby. An image is worth 16x16 words: Transformers for image recognition at scale. *ICLR*, 2021. 3
- [17] Andreas Doumanoglou, Rigas Kouskouridas, Sotiris Malassiotis, and Tae-Kyun Kim. Recovering 6D object pose and predicting next-best-view in the crowd. *CVPR*, 2016. 5
- [18] Bertram Drost, Markus Ulrich, Paul Bergmann, Philipp Hartinger, and Carsten Steger. Introducing MVTec ITODD – A dataset for 3D object recognition in industry. *ICCVW*, 2017. 5
- [19] Olivier Faugeras and M. Hebert. The representation, recognition, and locating of 3-D objects. *IJRR*, 1986. 2
- [20] M. A. Fischler and R. C. Bolles. Random sample consensus: A paradigm for model fitting with applications to image analysis and automated cartography. *Communications of the ACM*, 1981. 2, 3, 5
- [21] Hugo Germain, Guillaume Bourmaud, and Vincent Lepetit. S2DNet: Learning accurate correspondences for sparse-to-dense feature matching. *ECCV*, 2020. 8
- [22] Rohit Girdhar, Alaaeldin El-Nouby, Zhuang Liu, Mannat Singh, Kalyan Vasudev Alwala, Armand Joulin, and Ishan Misra. ImageBind: One embedding space to bind them all. *CVPR*, 2023. 3
- [23] Walter Goodwin, Sagar Vaze, Ioannis Havoutis, and Ingmar Posner. Zero-shot category-level object pose estimation. *ECCV*, 2022. 2, 3
- [24] Yang Hai, Rui Song, Jiaojiao Li, and Yinlin Hu. Shape-Constraint Recurrent Flow for 6D Object Pose Estimation. *CVPR*, 2023. 2
- [25] Kaiming He, Georgia Gkioxari, Piotr Dollár, and Ross Girshick. Mask R-CNN. *ICCV*, 2017. 2, 5
- [26] Xingyi He, Jiaming Sun, Yuang Wang, Di Huang, Hujun Bao, and Xiaowei Zhou. OnePose++: Keypoint-free one-shot object pose estimation without CAD models. *NeurIPS*, 2022. 2
- [27] Yisheng He, Yao Wang, Haoqiang Fan, Jian Sun, and Qifeng Chen. FS6D: Few-shot 6D pose estimation of novel objects. *CVPR*, 2022. 2
- [28] Stefan Hinterstoisser, Cedric Cagniart, Slobodan Ilic, Peter Sturm, Nassir Navab, Pascal Fua, and Vincent Lepetit. Gradient response maps for real-time detection of textureless objects. *TPAMI*, 2012. 2
- [29] Stefan Hinterstoisser, Vincent Lepetit, Slobodan Ilic, Pascal Fua, and Nassir Navab. Dominant orientation templates for real-time detection of texture-less objects. *CVPR*, 2010. 1, 2
- [30] Tomas Hodan, Daniel Barath, and Jiri Matas. EPOS: Estimating 6D pose of objects with symmetries. *CVPR*, 2020. 2, 5
- [31] Tomas Hodan, Pavel Haluza, Stepan Odrzalek, Jiri Matas, Manolis Lourakis, and Xenophon Zabulis. T-LESS: An RGB-D dataset for 6D pose estimation of texture-less objects. *WACV*, 2017. 4, 5
- [32] Tomas Hodan, Frank Michel, Eric Brachmann, Wadim Kehl, Anders Glent Buch, Dirk Kraft, Bertram Drost, Joel Vidal, Stephan Ihrke, Xenophon Zabulis, Caner Sahin, Fabian Manhardt, Federico Tombari, Tae-Kyun Kim, Jiri Matas, and Carsten Rother. BOP: Benchmark for 6D object pose estimation. *ECCV*, 2018. 2, 5
- [33] Tomas Hodan, Martin Sundermeyer, Bertram Drost, Yann Labbé, Eric Brachmann, Frank Michel, Carsten Rother, and Jiri Matas. BOP challenge 2020 on 6D object localization. *ECCVW*, 2020. 2, 5
- [34] Tomas Hodan, Martin Sundermeyer, Yann Labbe, Gu Wang, Eric Brachmann, Bertram Drost, Carsten Rother, and Jiri Matas. BOP challenge 2023 on detection, segmentation and pose estimation of unseen rigid objects. *To be published.*, 2023. The results are available at bop.felk.cvut.cz. 2, 5, 7
- [35] Yinlin Hu, Joachim Hugonot, Pascal Fua, and Mathieu Salzmann. Segmentation-driven 6D object pose estimation. *CVPR*, 2019. 2

- [36] Daniel P. Huttenlocher and Shimon Ullman. Recognizing solid objects by alignment with an image. *IJCV*, 1990. 2
- [37] Chao Jia, Yinfei Yang, Ye Xia, Yi-Ting Chen, Zarana Parekh, Hieu Pham, Quoc V. Le, Yunhsuan Sung, Zhen Li, and Tom Duerig. Scaling up visual and vision-language representation learning with noisy text supervision. *ICML*, 2021. 2, 3
- [38] Roman Kaskman, Sergey Zakharov, Ivan Shugurov, and Slobodan Ilic. HomebrewedDB: RGB-D dataset for 6D pose estimation of 3D objects. *ICCVW*, 2019. 5
- [39] Wadim Kehl, Fabian Manhardt, Federico Tombari, Slobodan Ilic, and Nassir Navab. SSD-6D: Making RGB-based 3D detection and 6D pose estimation great again. *ICCV*, 2017. 2
- [40] Alexander Kirillov, Eric Mintun, Nikhila Ravi, Hanzi Mao, Chloe Rolland, Laura Gustafson, Tete Xiao, Spencer Whitehead, Alexander C. Berg, Wan-Yen Lo, Piotr Dollár, and Ross Girshick. Segment anything. *ICCV*, 2023. 2, 8
- [41] Yann Labbé, Lucas Manuelli, Arsalan Mousavian, Stephen Tyree, Stan Birchfield, Jonathan Tremblay, Justin Carpentier, Mathieu Aubry, Dieter Fox, and Josef Sivic. MegaPose: 6D pose estimation of novel objects via render & compare. *CoRL*, 2022. 2, 5, 7
- [42] Yann Labbé, Justin Carpentier, Mathieu Aubry, and Josef Sivic. CosyPose: Consistent multi-view multi-object 6D pose estimation. *ECCV*, 2020. 2
- [43] Vincent Lepetit, Francesc Moreno-Noguer, and Pascal Fua. EPnP: An accurate $O(n)$ solution to the PnP problem. *IJCV*, 2009. 2, 3, 5
- [44] Kenneth Levenberg. A method for the solution of certain non-linear problems in least squares. *Quarterly of Applied Mathematics*, 1944. 5
- [45] Yi Li, Gu Wang, Xiangyang Ji, Yu Xiang, and Dieter Fox. DeepIM: Deep iterative matching for 6D pose estimation. *IJCV*, 2020. 2
- [46] Zhigang Li, Gu Wang, and Xiangyang Ji. CDPN: Coordinates-based disentangled pose network for real-time RGB-based 6-DoF object pose estimation. *ICCV*, 2019. 2
- [47] Yuan Liu, Yilin Wen, Sida Peng, Cheng Lin, Xiaoxiao Long, Taku Komura, and Wenping Wang. Gen6D: Generalizable model-free 6-DoF object pose estimation from RGB images. *ECCV*, 2022. 2
- [48] Yang Liu, Muzhi Zhu, Hengtao Li, Hao Chen, Xinlong Wang, and Chunhua Shen. Matcher: Segment anything with one shot using all-purpose feature matching. *arXiv preprint arXiv:2305.13310*, 2023. 3
- [49] David G. Lowe. *Perceptual Organization and Visual Recognition*. The Kluwer International Series in Engineering and Computer Science. Springer US, 1985. 2
- [50] David G Lowe. Three-dimensional object recognition from single two-dimensional images. *Artificial Intelligence*, 1987. 1, 2
- [51] David G. Lowe. Object recognition from local scale-invariant features. *ICCV*, 1999. 2
- [52] David G Lowe. Distinctive image features from scale-invariant keypoints. *IJCV*, 2004. 8
- [53] Fabian Manhardt, Wadim Kehl, Nassir Navab, and Federico Tombari. Deep Model-Based 6D Pose Refinement in RGB. *ECCV*, 2018. 2
- [54] Donald W. Marquardt. An algorithm for least-squares estimation of nonlinear parameters. *Journal of the Society for Industrial and Applied Mathematics*, 1963. 5
- [55] Jiri Matas, Ondrej Chum, Martin Urban, and Tomas Pajdla. Robust wide-baseline stereo from maximally stable extremal regions. *BMCV*, 2002. 2
- [56] Luke Melas-Kyriazi, Christian Rupprecht, Iro Laina, and Andrea Vedaldi. Deep spectral methods: A surprisingly strong baseline for unsupervised semantic segmentation and localization. *CVPR*, 2022. 2, 3
- [57] Sungphill Moon and Hyeontae Son. GenFlow, a submission to the BOP Challenge 2023 (bop.felk.cvut.cz). *Unpublished*, 2023. 2, 5, 7
- [58] Hiroshi Murase and Shree K. Nayar. Visual learning and recognition of 3-D objects from appearance. *IJCV*, 1995. 1, 2
- [59] Richard A Newcombe, Shahram Izadi, Otmar Hilliges, David Molyneaux, David Kim, Andrew J Davison, Pushmeet Kohi, Jamie Shotton, Steve Hodges, and Andrew Fitzgibbon. KinectFusion: Real-time dense surface mapping and tracking. *ISMAR*, 2011. 1
- [60] Van Nguyen Nguyen, Thibault Groueix, Georgy Ponimatin, Vincent Lepetit, and Tomas Hodan. CNOS: A strong baseline for CAD-based novel object segmentation. *ICCVW*, 2023. 2, 3, 5, 8
- [61] Van Nguyen Nguyen, Yinlin Hu, Yang Xiao, Mathieu Salzmann, and Vincent Lepetit. Templates for 3D object pose estimation revisited: Generalization to new objects and robustness to occlusions. *CVPR*, 2022. 2
- [62] Markus Oberweger, Paul Wohlhart, and Vincent Lepetit. Training a feedback loop for hand pose estimation. *ICCV*, 2015. 2
- [63] Brian Okorn, Qiao Gu, Martial Hebert, and David Held. ZePHYR: Zero-shot pose hypothesis rating. *ICRA*, 2021. 2
- [64] Clark F. Olson and Daniel P. Huttenlocher. Automatic target recognition by matching oriented edge pixels. *IEEE Transactions on Image Processing*, 1997. 2
- [65] Maxime Oquab, Timothée Darcet, Théo Moutakanni, Huy Vo, Marc Szafraniec, Vasil Khalidov, Pierre Fernandez, Daniel Haziza, Francisco Massa, Alaaeldin El-Nouby, et al. DINOv2: Learning robust visual features without supervision. *arXiv preprint arXiv:2304.07193*, 2023. 2, 3
- [66] Evin Pınar Örnek, Aravindhan K Krishnan, Shreekanth Gayaka, Cheng-Hao Kuo, Arnie Sen, Nassir Navab, and Federico Tombari. SuperRGB-D: Zero-shot instance segmentation in cluttered indoor environments. *IEEE RA-L*, 2023. 3
- [67] Keunhong Park, Arsalan Mousavian, Yu Xiang, and Dieter Fox. LatentFusion: End-to-end differentiable reconstruction and rendering for unseen object pose estimation. *CVPR*, 2020. 2
- [68] Kiru Park, Timothy Patten, and Markus Vincze. Pix2Pose: Pixel-wise coordinate regression of objects for 6D pose estimation. *ICCV*, 2019. 2
- [69] Georgios Pavlakos, Xiaowei Zhou, Aaron Chan, Konstantinos G. Derpanis, and Kostas Daniilidis. 6-DoF object pose from semantic keypoints. *ICRA*, 2017. 2
- [70] Sida Peng, Yuan Liu, Qixing Huang, Hujun Bao, and Xiaowei Zhou. PVNet: Pixel-wise voting network for 6DoF pose estimation. *CVPR*, 2019. 2
- [71] James Philbin, Ondrej Chum, Michael Isard, Josef Sivic, and Andrew Zisserman. Object retrieval with large vocabularies and fast spatial matching. *CVPR*, 2007. 4
- [72] James Philbin, Ondrej Chum, Michael Isard, Josef Sivic, and Andrew Zisserman. Lost in quantization: Improving particular object retrieval in large scale image databases. *CVPR*, 2008. 4
- [73] Giorgia Pitteri, Aurélie Bugeau, Slobodan Ilic, and Vincent Lepetit. 3D object detection and pose estimation of unseen objects in color images with local surface embeddings. *ACCV*, 2020. 2
- [74] Giorgia Pitteri, Slobodan Ilic, and Vincent Lepetit. CorNet: Generic 3D corners for 6D pose estimation of new objects without retraining. *ICCVW*, 2019. 2

- [75] Alec Radford, Jong Wook Kim, Chris Hallacy, Aditya Ramesh, Gabriel Goh, Sandhini Agarwal, Girish Sastry, Amanda Askell, Pamela Mishkin, Jack Clark, Gretchen Krueger, and Ilya Sutskever. Learning transferable visual models from natural language supervision. *ICML*, 2021. [2](#), [3](#), [8](#)
- [76] Jeremy Reizenstein, Roman Shapovalov, Philipp Henzler, Luca Sbordone, Patrick Labatut, and David Novotny. Common objects in 3D: Large-scale learning and evaluation of real-life 3D category reconstruction. *ICCV*, 2021. [1](#)
- [77] Lawrence G Roberts. *Machine perception of three-dimensional solids*. PhD thesis, Massachusetts Institute of Technology, 1963. [1](#), [2](#)
- [78] F. Rothganger, S. Lazebnik, C. Schmid, and J. Ponce. 3D object modeling and recognition using affine-invariant patches and multi-view spatial constraints. *CVPR*, 2003. [1](#), [2](#)
- [79] Paul-Edouard Sarlin, Ajaykumar Unagar, Måns Larsson, Hugo Germain, Carl Toft, Victor Larsson, Marc Pollefeys, Vincent Lepetit, Lars Hammarstrand, Fredrik Kahl, and Torsten Sattler. Back to the feature: Learning robust camera localization from pixels to pose. *CVPR*, 2021. [5](#)
- [80] Christoph Schuhmann, Romain Beaumont, Richard Vencu, Cade W Gordon, Ross Wightman, et al. LAION-5B: An open large-scale dataset for training next generation image-text models. *NeurIPS Datasets and Benchmarks Track*, 2022. [3](#)
- [81] Dave Shreiner. *OpenGL programming guide: the official guide to learning OpenGL, versions 3.0 and 3.1*. Pearson Education, 2009. [4](#)
- [82] Ivan Shugurov, Fu Li, Benjamin Busam, and Slobodan Ilic. OSOP: A multi-stage one shot object pose estimation framework. *CVPR*, 2022. [2](#), [5](#), [7](#)
- [83] Oriane Siméoni, Gilles Puy, Huy V. Vo, Simon Roburin, Spyros Gidaris, Andrei Bursuc, Patrick Pérez, Renaud Marlet, and Jean Ponce. Localizing objects with self-supervised transformers and no labels. *BMVC*, 2021. [3](#)
- [84] Sivic and Zisserman. Video Google: A text retrieval approach to object matching in videos. *ICCV*, 2003. [2](#), [4](#)
- [85] Chen Song, Jiaru Song, and Qixing Huang. HybridPose: 6D Object Pose Estimation under Hybrid Representations. *CVPR*, 2020. [2](#)
- [86] Jiaming Sun, Zehong Shen, Yuang Wang, Hujun Bao, and Xiaowei Zhou. LoFTR: Detector-free local feature matching with transformers. *CVPR*, 2021. [8](#)
- [87] Jiaming Sun, Zihao Wang, Siyu Zhang, Xingyi He, Hongcheng Zhao, Guofeng Zhang, and Xiaowei Zhou. OnePose: One-shot object pose estimation without CAD models. *CVPR*, 2022. [2](#)
- [88] Martin Sundermeyer, Maximilian Durner, En Yen Puang, Zoltan-Csaba Marton, Narunas Vaskevicius, Kai O. Arras, and Rudolph Triebel. Multi-path learning for object pose estimation across domains. *CVPR*, 2020. [2](#)
- [89] Martin Sundermeyer, Tomas Hodan, Yann Labbé, Gu Wang, Eric Brachmann, Bertram Drost, Carsten Rother, and Jiri Matas. BOP challenge 2022 on detection, segmentation and pose estimation of specific rigid objects. *CVPRW*, 2023. [1](#), [2](#), [5](#), [7](#)
- [90] Martin Sundermeyer, Zoltan-Csaba Marton, Maximilian Durner, Manuel Brucker, and Rudolph Triebel. Implicit 3D orientation learning for 6D object detection from rgb images. *ECCV*, 2018. [2](#)
- [91] Bugra Tekin, Sudipta N. Sinha, and Pascal Fua. Real-time seamless single shot 6D object pose prediction. *CVPR*, 2018. [2](#)
- [92] Stefan Thalhammer, Jean-Baptiste Weibel, Markus Vincze, and Jose Garcia-Rodriguez. Self-supervised vision transformers for 3D pose estimation of novel objects. *arXiv preprint arXiv:2306.00129*, 2023. [2](#)
- [93] Federico Tombari, Alessandro Franchi, and Luigi Di. BOLD features to detect texture-less objects. *ICCV*, 2013. [2](#)
- [94] Akihiko Torii, Josef Sivic, Tomas Pajdla, and Masatoshi Okutomi. Visual place recognition with repetitive structures. *CVPR*, 2013. [4](#)
- [95] Lukas von Stumberg, Patrick Wenzel, Nan Yang, and Daniel Cremers. LM-Reloc: Levenberg-Marquardt based direct visual relocalization. *3DV*, 2020. [5](#)
- [96] Gu Wang, Fabian Manhardt, Federico Tombari, and Xiangyang Ji. GDR-Net: Geometry-guided direct regression network for monocular 6D object pose estimation. *CVPR*, 2021. [2](#)
- [97] Yangtao Wang, Xi Shen, Shell Hu, Yuan Yuan, James Crowley, and Dominique Vaufreydaz. Self-supervised transformers for unsupervised object discovery using normalized cut. *CVPR*, 2022. [2](#), [3](#)
- [98] Paul Wohlhart and Vincent Lepetit. Learning descriptors for object recognition and 3D pose estimation. *CVPR*, 2015. [2](#)
- [99] Chao-Yuan Wu, Justin Johnson, Jitendra Malik, Christoph Feichtenhofer, and Georgia Gkioxari. Multiview compressive coding for 3D reconstruction. *CVPR*, 2023. [1](#)
- [100] Yu Xiang, Tanner Schmidt, Venkatraman Narayanan, and Dieter Fox. PoseCNN: A convolutional neural network for 6D object pose estimation in cluttered scenes. *RSS*, 2018. [2](#), [4](#), [5](#)
- [101] Yang Xiao, Xuchong Qiu, Pierre-Alain Langlois, Mathieu Aubry, and Renaud Marlet. Pose from shape: Deep pose estimation for arbitrary 3D objects. *BMVC*, 2019. [2](#)
- [102] Sergey Zakharov, Ivan Shugurov, and Slobodan Ilic. DPOD: 6D Pose Object Detector and Refiner. *ICCV*, 2019. [2](#)
- [103] Junyi Zhang, Charles Herrmann, Junhwa Hur, Luisa Polania Cabrera, Varun Jampani, Deqing Sun, and Ming-Hsuan Yang. A tale of two features: Stable diffusion complements DINO for zero-shot semantic correspondence. *NeurIPS*, 2023. [3](#)
- [104] Jinghao Zhou, Chen Wei, Huiyu Wang, Wei Shen, Cihang Xie, Alan Yuille, and Tao Kong. iBOT: Image BERT pre-training with online tokenizer. *ICLR*, 2022. [3](#)